Xue, Bing; Haneda, Katsuyuki; Icheln, Clemens

Improving the Patch based Crossovers by Parasitic Modes and a Sub-element Technique

Published in:
IEEE Transactions on Circuits and Systems II: Express Briefs

DOI:
10.1109/TCSII.2022.3177928

Published: 01/09/2022

Document Version
Peer-reviewed accepted author manuscript, also known as Final accepted manuscript or Post-print

Please cite the original version:
Xue, B., Haneda, K., & Icheln, C. (2022). Improving the Patch based Crossovers by Parasitic Modes and a Sub-element Technique. *IEEE Transactions on Circuits and Systems II: Express Briefs*, *69*(9), 3774-3778. https://doi.org/10.1109/TCSII.2022.3177928

Improving the Patch based Crossovers by Parasitic Modes and a Sub-element Technique

Bing Xue, Katsuyuki Haneda, *Member, IEEE*, and Clemens Icheln

***Abstract*—This brief introduces new methodologies to design microstrip line crossovers on a high-speed interconnection circuit. The crossover is based on a simple square patch, which employs TM_{100} and TM_{001} to achieve mode orthogonality so that two sets of intersecting signals can transmit along microstrip lines with a high isolation. Compared with rectangular waveguide crossovers that employ high modes, namely TE_{102} and TE_{201}, it shows advantages like a smaller size and easier manufacturing. Then, the relevant techniques for performance improvement, including radiation suppression and bandwidth widening, are studied for practical circuit designs. Finally, based on the sub-element technique, the study designs a controllable frequency response for two intersecting signals and miniaturization of patch based crossovers. Two examples are implemented, manufactured and measured to justify the validity of the sub-element technology. In addition, the design steps of this method are simplified compared with relying on full-wave simulations entirely.**

***Index Terms*—patch-based crossover, bandpass responses, controllable frequency, sub-element technology, bandwidth widening.**

I. Introduction

Microwave communication systems are becoming increasingly complex in order to meet user requirements, namely multi-functions such as filtering, miniaturization, and cost effectiveness [1]- [5]. With this trend, intersecting lines can be easily seen in many systems because of limited spaces. In order to use a single layer to arrange all transmission lines, crossovers as a kind of useful components have been proposed to solve this issue in high-speed interconnection circuits [5]. Because of the diversity of circuit types, multi-functional crossovers have been proposed, especially crossovers with filtering features [3]–[12]. For instance, in [3], the authors designed a single-layer single-ended-to-balanced crossover which can present an excellent common-mode suppression; [4] utilized mode coupling methods to create a wide bandwidth crossover based on the Substrate Integrated Waveguide (SIW). Later on, the work in [5] proposed SIW based crossover using orthogonal degenerate modes. This crossover can work in a narrow bandwidth but with an excellent isolation; [6] showed a crossover similar to the one in [5] but with vias to increase resonance frequencies and to broaden the bandwidth. In addition, [7] widened the bandwidth of the SIW-based crossover using an increased resonance waveguide mode to couple the TE_{201} and TE_{102} modes. Differing from the traditional methods to design crossovers, filtering crossovers can provide two sets of intersecting signals, one with the same bandpass responses and the other with different bandpass responses; [8], [9] brought in a filtering crossover concept and extended the two-channel crossovers to multi-channel. It is worth mentioning that the authors in [8] changed the current paths to make the frequencies controllable. Similarly, [10], [11] continued to use the filtering crossover concept and adopted a method similar to that in [7] to control transmission frequencies. Different from the methods in [6], [7], the work [12], [13] used the extra coplanar waveguide modes to broaden the bandwidth, allowing miniaturization. However, these existing works increase the complexity of circuit structures and manufacturing because of the need of an excessive amount of vias and large footprint. Therefore, [14], [15] presented a simpler structure to generate orthogonal modes, based on square patch, which opened a new door for crossovers.

In this brief, similar to [15], low-order orthogonal modes are, firstly, applied to filtering crossovers to create a simple and easy-to-integrate structure while achieving a suitable performance. Then, in order to reduce the radiation loss of the patch and widen the bandwidth of bandpass response, a new mode near the main mode is added by parasitic coplanar waveguides. The new mode generates a favorable resonance between isolated ports and changes the current distributions on patches. In this way, the performance of patch based crossover is improved significantly. Then, by using the sub-element technology [16]–[18], the patch based crossovers is miniaturized while a frequency response can be controlled for two intersecting signals. With one-time electromagnetic simulation and several-time circuit simulations, the required designs can be easily achieved.

This brief's innovations can be summarized as the following three points:

1) the center-feeding patch based crossovers, along with a formula for bandwidth estimation is derived.
2) the improvement of the patch based crossovers by parasitic modes generated by co-planer waveguides.
3) the improvement of the patch based crossover design using the sub-element technique.

II. Patch-based Crossover

A. Fundamental Theory of Patch based Crossover

Crossovers based on orthogonal modes have been proposed for many years [5]. SIW resonators are being used to generate orthogonal modes in planer circuits [4]–[12]. A notable problem in the SIW technique, however, is that the need of many vias as

Manuscript created January 18, 2022; revised xx, xx; accepted xx xx. Date of publication xx; date of current version xx xx, xx. B. Xue, K. Haneda and C. Icheln are with the Department of Electronics and Nanoengineering, Aalto University-School of Electrical Engineering, Espoo FI-00076, Finland. (Corresponding author: Bing Xue.(e-mail: Bing.Xue@aalto.fi))

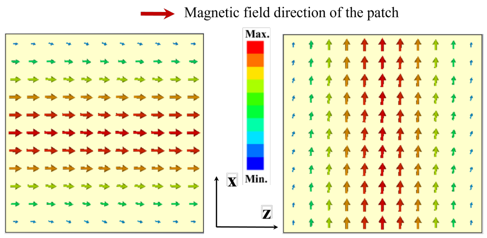

Fig. 1: TM_{100} and TM_{001} of a square patch

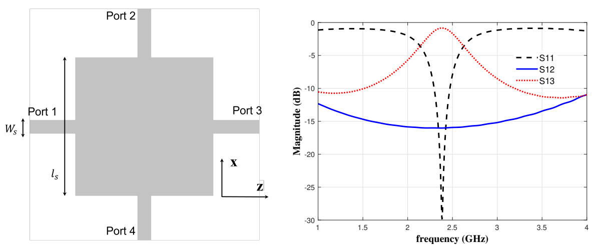

(a) (b)

Fig. 2: (a) A classical patch crossover ($W_s = 2.87$ mm, $l_s = 30$ mm) and (b) S_{11}, S_{12} and S_{13} of patch crossover

the metal walls of resonators that increases the manufacturing complexity and cost. Instead of using vias, open structures can be used as the resonators for generating orthogonal modes. The boundary of patch antennas can be regarded as the open circuit while the boundary of SIW based resonators can be seen as the short circuit. Accordingly, a square patch is applied as a resonator in the crossover where the fundamental mode is TM_{100} and TM_{001} as Fig.1 shows. These two modes are orthogonal, creating a high isolation for the two intersecting transmission lines. The magnetic (H) fields inside resonators can be represented regarding TM_{m0n} modes as:

$$\begin{aligned} H_x &= A_1 \cos(m\pi x/l_s) \sin(n\pi x/l_s) \\ H_z &= A_1 \sin(m\pi x/l_s) \cos(n\pi x/l_s) \end{aligned} \tag{1}$$

where m and n are the mode numbers and A_1 is the amplitude of the fields and l_s is the length of a square patch. The resonance frequency can be determined by [14]

$$f_0 = \frac{c}{2l_s\sqrt{\epsilon_r}} \tag{2}$$

where ϵ_r is the substrate's,in practice, microstrip lines' effective dielectric constant and c is the light speed in free space. Because the patch can be seen as a half-wave transmission line along the transmission direction, the fractional bandwidth of a patch crossover can be represented by

$$\frac{\Delta f}{f_0} = \frac{2}{\pi}\cot^{-1}\left[\frac{\sqrt{(z^2-1)^2 - |\Gamma_m|^2 (z^2+1)^2}}{2z|\Gamma_m|}\right] \tag{3}$$

where z is the normalized impedance of the patch (Z_c) to reference impedance (Z_0); Γ_m is for an acceptable reflection coefficient; Z_c can be computed by the microstrip line.

B. Transmission Performance

To justify the performance of patch based crossovers, microstrip lines are used to connect the square patch. In addition, in the following simulations, 1.5 mm-thickness FR4 substrates (dielectric constant: 4.3, loss tangent: 0.02) are employed. The design frequency range is from 1.5 GHz to 2.5 GHz. The metal is copper with 0.035 mm thickness. Then, a simple example

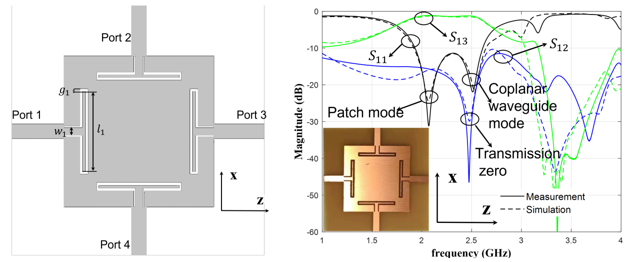

(a) (b)

Fig. 3: (a) Patch crossover with a coplanar waveguide mode ($W_1 = 1.50$ mm, $g_0 = 0.50$ mm). and (b) S_{11}, S_{12} and S_{13} of patch crossover with a coplanar waveguide mode

is demonstrated to study the transmission performance of the patch based crossover. As Fig.2 (a) shows, $W_s = 2.87$ mm is the 50Ω microstrip line's width and $l_s = 30$ mm is the length of the square patch. By full-wave electromagnetic simulation, it is easy to obtain the S parameters of 4 ports. Because this structure is symmetrical and reciprocal and the 4 ports are identical, S_{11}, S_{12} and S_{13} are shown in Fig.2 (b). The center frequency f_0 is 2.37 GHz with -10 dB bandwidth from 2.29 GHz to 2.47 GHz; S_{13} shows the transmission loss of 1.6 dB while S_{12} indicates an isolation of 15 dB across the bandwidth; the transmission loss is mainly because of the radiation of the patch and the dielectric loss.

C. Performance Improvement of Patch based Crossover

In the previous section, a simple patch crossover shows a narrow bandwidth and obvious transmission loss in bandwidth. In this section, a technique to improve bandwidth and reduce radiation loss is proposed. In [12], the authors introduced an extra transmission mode to broaden the bandwidth of SIW crossovers near the main mode. Similar to this idea, a parasitic coplanar waveguide mode is proposed as shown in Fig.3 (a). In order to study transmission characteristics, full wave electromagnetic simulations are operated, resulting in S parameters shown in Fig.3 (b). There are two resonances in the transmission bandwidth of S_{11}. They are created by two modes, namely patch mode (TM_{001}) and coplanar waveguide mode, which widen the bandwidth. Differing from [15], the coplanar waveguide modes are coupled to each other directly as shown in Fig.4, which is why there are only two resonances. Moreover, the transmission loss is 1.2 dB and is reduced by 0.4 dB compared to the simple patch crossover in Fig.2 because the radiation loss is reduced. Then, the isolation between port 1 and port 2 is improved because a transmission zero is brought in as Fig.3 (b) shows. By observing the electric fields in two resonating modes, 2.06 GHz as the patch mode and 2.50 GHz as the coplanar waveguide mode are presented in Fig.4. The patch mode is shifted to the low frequency, compared with simple patch crossovers shown in Fig.2 (a), because the coplanar waveguide increases current paths [8]. The third resonance can be found at around 3.2 GHz, which radiates power rather than transmitting power to other ports. Accordingly, this mode cannot be used to improve the performance of the crossover. Finally, in order to validate the simulation, a prototype with the same parameters of simulations is manufactured and S parameters are measured by a vector network analyser (VNA). In Fig.3 (b), S parameters of measurements show a close agreement with simulations, though the slight difference between them is because of manufacture errors and SMA connector impacts. It was thereby verified that the proposed crossover presents a lower radiation loss, a higher isolation, and a wider band than the existing designs.

III. The Use of Sub-element Technique for Improved Crossovers

In order to improve the patch based crossover further, a sub-element technique is introduced in this section. The technique allows us to design crossovers according to user-defined requirements of S parameters.

A. Theory of Sub-element Technique

Previous works apply the sub-element technique to make antennas miniaturized and behaving as a filter [16]–[18]. In this section, the technique is applied to the patch crossover design. A patch can be divided into several small sub-elements, shown in Fig.5 (a). All sub-elements can be connected with neighboring sub-elements by hard wires. When it is assumed that all sub-elements are connected by ports in Fig.5 (a) and add 4 original ports, an impedance matrix can be obtained for each port as

$$\boldsymbol{U} = \boldsymbol{Z}\boldsymbol{I} \tag{4}$$

where $\boldsymbol{U}$ and $\boldsymbol{I}$ are N-element voltage and current matrix where N is the number of ports; $\boldsymbol{Z}$ can be written as

$$\boldsymbol{Z} = \begin{bmatrix} Z_{11} & \cdots & Z_{1N} \\ \vdots & \ddots & \vdots \\ Z_{N1} & \cdots & Z_{NN} \end{bmatrix} \tag{5}$$

where an element Z_{ij} denotes an impedance of port between j-th and i-th sub-element. When hard wires are used to replace ports, the related elements in $\boldsymbol{Z}$ should be 0. When the ports are set as the open circuit, the related elements in $\boldsymbol{Z}$ should be infinite. Then, we can use electromagnetic simulations to obtain the S parameters for all ports. By changing the new ports to 'open' and 'short' states, different transmission characteristics for original 4 ports can be obtained. Next, non-linear optimization methods, like the genetic algorithm, particle swarm optimization algorithm and some machine learning based methods, can be employed to find the best solutions for user-defined cost functions defining, e.g., required impedance and isolation bandwidth. Because crossovers are passive components, $S_{ab} = S_{ba}$ is fulfilled, where a and b are ranging from 1 to 4. The cost functions can be represented by, for example:

$$\begin{cases} S_{11}(f_1) < S^1, S_{33}(f_1) < S^1, \\ S_{22}(f_2) < S^2, S_{44}(f_2) < S^2, \\ S_{13}(f_1) > S^3, S_{24}(f_2) > S^4, \\ S_{12}(f_3) < S^5, S_{14}(f_3) < S^6, \\ S_{23}(f_3) < S^7, S_{34}(f_3) < S^8 \end{cases} \tag{6}$$

where f_1 is the frequency of interest for a signal path from port 1 to port 3, f_2 is the same from port 2 to port 4, f_3 is in $[f_1, f_2]$, S^1 and S^2 are the required level of reflection coefficients, S^3 and S^4 represent those of insertion loss, and finally S^5, S^6, S^7 and S^8 represent those for isolation coefficients. When

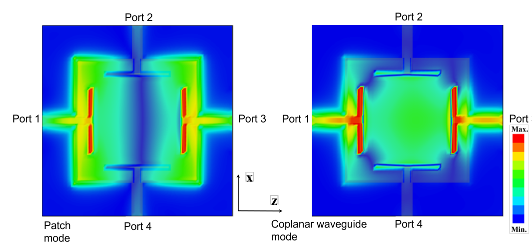

Fig. 4: Electric field distributions of patch mode (2.06 GHz) and coplanar waveguide mode (2.50 GHz)

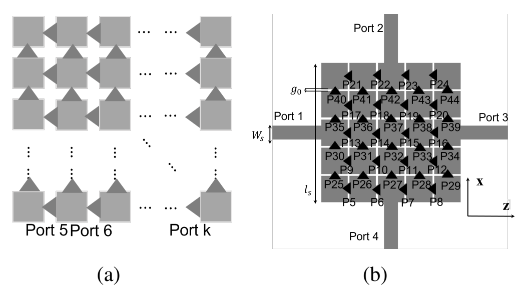

Fig. 5: (a) Sub-element patch with ports and (b) 25-element sub-element patch with 44 ports

non-linear optimization methods are employed to optimize crossovers, we optimize the value of all resistors either by 0 Ω or 10000 Ω to represent short and open ports, respectively. The sub-element technique can be solved as follows:

1) choose the patch size and the number of sub-elements and model them for full wave simulations
2) run full wave simulations and obtain S parameters for all ports
3) run circuit simulations by S parameter data and apply non-linear optimization to meet the cost functions.
4) use the states of all ports to modify the model of full wave simulations and run full wave simulation again to check if the cost functions are met.

During the design, it is worth noticing that, there are two important parameters, namely the gap (g_0) between adjacent sub-elements and the width (w_0) of hard wires to connect elements. For g_0, it does not influence the consistency between circuit simulation and full wave simulation since S parameters

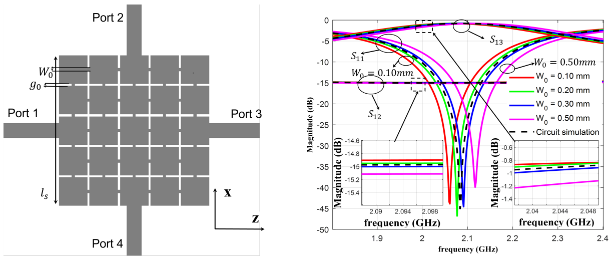

(a) (b)

Fig. 6: (a) A sub-element patch with full hard-wire connections and (b) S_{11}, S_{12} and S_{13} of a sub-element patch with full hard-wire connections

include influences from g_0. For w_0, it is an ideal feed line in circuit simulations while it is a w_0-width feed line in full wave simulations. Therefore, w_0 must be a defined value in practical designs. In order to study sub-element crossover performance, a 25-element example is shown in Fig.5 (b). In this case, the number of ports is 44, including 4 original ports; w_s is still the width of 50 Ω mircostrip lines, while g_0 is 0.5 mm and l_s is 30 mm as the classical patch-based crossover in Fig.2 (a). In the follow section, w_0's impacts on S parameters will be studied.

B. Parametric Study of Sub-element Crossovers

Firstly, hard wires are used to connect all sub-elements to their adjacent elements as Fig.6 (a) shows. Then, by changing the w_0, we find its effects on reflection coefficients in Fig.6 (b). The electromagnetic simulations needs several minutes for a single simulation while it takes several seconds to run circuit simulations. Then, by observing curves in Fig.6 (b), with w_0 increasing, the impedance bandwidth is shifted to the high frequency. It can be seen that $w_0 = 0.25$ mm is a value to make a close agreement between circuit and electromagnetic simulations. Therefore, in the following cases, $w_0 = 0.25$ mm is applied to electromagnetic simulations. It is worth mentioning that $w_0 = 0.25$ mm is an optimal value for this 25-sub-element crossover design and may not be so for other cases. Compared with the classical patch crossover and its S parameters in Fig.2 (b), the sub-element crossover can reach impedance matching at a lower frequency when the patches are with the same size. It is because the thin hard wires increase the current path lengths on the patch as illustrated [8].

C. Sub-element Crossovers with Different Operating Frequencies

Next, an example is shown here to show a sub-element crossover design. The requirements are defined as the following equations.

$$\begin{cases} S_{11}(f_1) < -10 \text{ dB}, S_{33}(f_1) < -10 \text{ dB}, \\ S_{22}(f_2) < -10 \text{ dB}, S_{44}(f_2) < -10 \text{ dB}, \\ S_{13}(f_1) > -2 \text{ dB}, S_{24}(f_2) > -2 \text{ dB}, \\ S_{12}(f_3) < -12 \text{ dB}, S_{14}(f_3) < -12 \text{ dB}, \\ S_{23}(f_3) < -12 \text{ dB}, S_{34}(f_3) < -12 \text{ dB} \end{cases} \tag{7}$$

where f_1 is from 1.9 GHz to 2.1 GHz, f_2 is from 2 GHz to 2.2 GHz and f_3 is from 1.9 GHz to 2.2 GHz. The weight of every equation in the target cost function (7) will influence the convergence of non-linear optimization. However, owing to fast speed of circuit simulations, weight of every equation can be set equally. In this example, the generic algorithm is employed to optimize the design. After solving the sub-element technique to obtain the state of each port, i.e., 0 or 10000 Ω, electromagnetic simulation is implemented. The optimized design of this crossover is shown in Fig.7 (a) where $w_0 = 0.25$ mm is adopted. From Fig.7 (a), three ports are opened while others are shorted. The reason of the frequency shift to the lower side for the transmission from Port 1 to Port 3 is the open ports that extended the current path length on the surrounding sub-elements. In Fig.7 (b), there is a close agreement among measurements, electromagnetic simulations and circuit simulation results. The insertion loss is about 1.9 dB at 2.0 GHz and 2.1 GHz for S_{13} and S_{24}, respectively, due to the dielectric loss. For lower insertion losses, substrates with smaller $\tan\delta$ should be chosen.

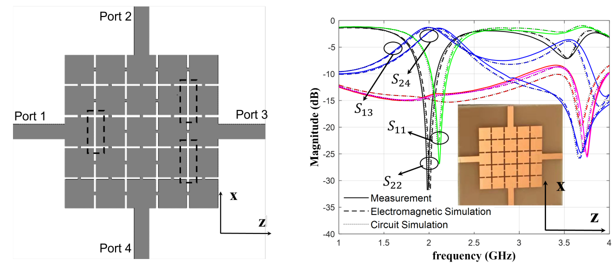

(a) (b)

Fig. 7: (a) A sub-element patch crossover with different operating frequencies and (b) S parameter comparisons of a sub-element patch crossover with different operating frequencies among measurements, electromagnetic simulations and circuit simulations

D. Sub-element Crossover with a Smaller Size

The second example is shown here to further verify the performance of the sub-element method. For this design, the requirements are defined as

$$\begin{cases} S_{11}(f_1) < -10 \text{ dB}, S_{33}(f_1) < -10 \text{ dB}, \\ S_{22}(f_2) < -10 \text{ dB}, S_{44}(f_2) < -10 \text{ dB}, \\ S_{13}(f_1) > -2.5 \text{ dB}, S_{24}(f_2) > -2.5 \text{ dB}, \\ S_{12}(f_3) < -12 \text{ dB}, S_{14}(f_3) < -12 \text{ dB}, \\ S_{23}(f_3) < -12 \text{ dB}, S_{34}(f_3) < -12 \text{ dB} \end{cases} \tag{8}$$

where f_1 is from 1.8 GHz to 2.0 GHz, f_2 is from 1.8 GHz to 2 GHz and f_3 is from 1.8 GHz to 2.0 GHz. Otherwise the same values and methods are used as the last example for optimization. Some elements in Fig.8 (a) have no connection with other elements and just contribute couplings to adjacent elements. From Fig.8 (b), the -10 dB impedance bandwidth of the realized crossover is nearly 200 MHz with a central frequency of 1.9 GHz. The insertion loss is about 1.6 dB at 1.9 GHz for S_{13} and about 1.8 dB at 1.9 GHz for S_{24}. The general level of isolation is 12 dB for all curves. The results from measurements, circuit simulations and electromagnetic simulations have a close agreement.

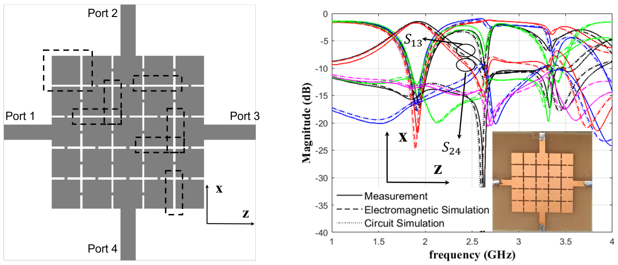

(a) (b)

Fig. 8: (a) A sub-element patch crossover with a smaller size and (b) S parameter comparisons of a sub-element patch crossover with a smaller size among measurements, electromagnetic simulations and circuit simulations

IV. Discussions

In order to discuss the performances of proposed designs, those from [5], [8] and [15] are compared with the work of this brief. Based on Table I, patch based crossovers show advantages in terms of manufacturing complexity, miniaturized size and transmission bandwidth. The coplanar waveguide mode further improves bandwidth and reduces the radiation loss. The sub-element technique makes the design process more flexible for various passband requirements. It is noticeable that sub-element technique may increase insertion losses of crossovers, because the thin hard wires increase the transmission paths of currents. However, for example, the use of more sub-elements and increasing widths of hard wires can mitigate the insertion loss.

TABLE I: Comparisons of crossover performances

Crossover Type	Size(λ_g^2)	CF	IL	FBW	MC
SIW [5]	1.44	No	0.5 dB	1.4%	high
CF-SIW [8]	3.98	Yes	1.75 dB	5.0%	high
patch [15]	0.48	No	0.5 dB	20%	low
patch (this work)	0.44	No	1.6 dB	20%	low
patch-coplanar (this work)	0.40	No	1.2 dB	32%	low
sub-element 1 (this work)	0.31	Yes	1.9 dB	$>20\%$	low
sub-element 2 (this work)	0.28	Yes	<1.8 dB	26%	low

CF is the controllable frequencies; IL is the insertion loss; FBW is the 3-dB frequency bandwidth; MC is the manufacturing complexity.

V. Conclusions

In this brief, a simple method to design good-performance patch crossovers is introduced, showing a smaller size than SIW based crossovers. Next, a coplanar waveguide mode is applied to broaden the bandwidth and reduce the radiation loss. Then, the sub-element technique is applied as a systematic approach to realize user-defined S parameter performance. The approach reduces the need of electromagnetic simulations that usually takes longer time than circuit simulations. The two design examples indicate validity of the approach. Finally, the manufactured crossovers show a very close agreement with circuit simulations and electromagnetic simulations.

References

[1] W. Feng, X. Ma, R. Gómez-García, Y. Shi, W. Che, and Q. Xue, “Multi-Functional Balanced-to-Unbalanced Filtering Power Dividers With Extended Upper Stopband,” *IEEE Transactions on Circuits and Systems II: Express Briefs*, vol.66,no.7,pp.1154–1158,Jul.2019..

[2] X. -K.Bi, T. Cheng, P. Cheong, S. -K.Ho, and K. -W.Tam, “Multi-Functional Balanced-to-Unbalanced Filtering Power Dividers With Extended Upper Stopband,” *IEEE Transactions on Circuits and Systems II: Express Briefs*, vol.66,no.3,pp.317–321,Mar.2019.

[3] Y. Zheng, W. Wang, Y. Wu and W. Chen, “A Single-Layer Planar Wideband Filtering Single-Ended-to-Balanced Crossover with Excellent Common-Mode Suppression,” *IEEE Transactions on Circuits and Systems II: Express Briefs*, doi: 10.1109/TCSII.2021.3100334.

[4] Y. Cao, Y. Wu, Z. Jiang and Z. Hao, “A Compact Millimeter-Wave Planar Directional Coupled Crossover With a Wide Bandwidth,” *IEEE Microwave and Wireless Components Letters*, vol. 30, no. 7, pp. 661-664, July 2020.

[5] S. Han, K. Zhou, J. Zhang, C. Zhou and W. Wu, “Novel Substrate Integrated Waveguide Filtering Crossover Using Orthogonal Degenerate Modes,” *IEEE Microwave and Wireless Components Letters*, vol. 27, no. 9, pp. 803-805, Sept. 2017.

[6] S. S. Hesari and J. Bornemann, “Substrate integrated waveguide crossover formed by orthogonal TE102 resonators,” *2017 47th European Microwave Conference (EuMC)*, 2017, pp. 17-20.

[7] Y. Zhou, K. Zhou, J. Zhang, C. Zhou and W. Wu, “Miniaturized substrate integrated waveguide filtering crossover,” *2017 IEEE Electrical Design of Advanced Packaging and Systems Symposium (EDAPS)*, 2017, pp. 1-3.

[8] W. -L. Zhan, J. -X. Xu, X. -L. Zhao, B. -J. Hu and X. Y. Zhang, “Substrate Integrated Waveguide Multi-Channel Filtering Crossover With Extended Channel Number and Controllable Frequencies,” *IEEE Transactions on Circuits and Systems II: Express Briefs*, vol. 67, no. 12, pp. 2858-2862, Dec. 2020.

[9] K. Zhou and K. Wu, “Multi-Channel SIW Filtering Crossover With Flexibly Specified Frequencies and Bandwidths,” *2020 IEEE USNC-CNC-URSI North American Radio Science Meeting (Joint with AP-S Symposium*, 2020, pp. 117-118.

[10] Y. Zhou, K. Zhou, J. Zhang, and W. Wu, “Substrate-integrated waveguide filtering crossovers with improved selectivity,” *International Journal of RF and Microwave Computer-Aided Engineering*, vol. 30, no. 3, Mar. 2020, Art. no. e22067.

[11] K. Zhou and K. Wu, “Wide-Stopband Substrate-Integrated Waveguide Filtering Crossovers With Flexibly Allocated Channel Frequencies and Bandwidths,” *IEEE Transactions on Microwave Theory and Techniques*, vol. 69, no. 7, pp. 3264-3274, July 2021.

[12] K. Zhou and K. Wu, “Compact Substrate-Integrated Waveguide Filtering Crossover by Embedding CPW Quarter-Wavelength Resonators,” *2020 IEEE/MTT-S International Microwave Symposium (IMS)*, 2020, pp. 916-919.

[13] L. Sun, H.-W. Deng, Y.-F. Xue, J.-M. Zhu, and S.-B. Xing, “Compact balanced BPF and filtering crossover with intrinsic common-mode suppression using single-layered SIW cavity,” *IEEE Microwave and Wireless Components Letters*, vol. 30, no. 2, pp. 144–147, Feb. 2020.

[14] A. Abbosh, “Planar Wideband Crossover with Distortionless Response using Dual-mode Microstrip Patch.,” *IET Microwave and Optical Technology Letters*, vol. 54, no. 9, pp. 2077-2079, 2012.

[15] B. Henin and A. Abbosh, “Design of compact planar crossover using Sierpinski carpet microstrip patch,” *IET Microwaves, Antennas Propagation*, vol. 7, no. 1, pp. 54-60, 2013.

[16] S. Song and R. D. Murch, “An Efficient Approach for Optimizing Frequency Reconfigurable Pixel Antennas Using Genetic Algorithms,” *IEEE Transactions on Antennas and Propagation*, vol. 62, no. 2, pp. 609-620, Feb. 2014.

[17] F. Jiang, C. -Y. Chiu, S. Shen, Q. S. Cheng and R. Murch, “Pixel Antenna Optimization Using N -Port Characteristic Mode Analysis,” *IEEE Transactions on Antennas and Propagation*, vol. 68, no. 5, pp. 3336-3347, May 2020.

[18] Fan Jiang, Shanpu Shen, Chi-Yuk Chiu, Zhen Zhang, Yujie Zhang, Qingsha S. Cheng, Ross Murch, ”Pixel Antenna Optimization Based on Perturbation Sensitivity Analysis”, *IEEE Transactions on Antennas and Propagation*, vol. 70, no. 1, pp. 472-486, 2022.